Journal of the European Ceramic Society 22 (2002) 511–520

www.elsevier.com/locate/jeurceramsoc

Formation of hydroxyapatite on $CaSiO_3$ powders in simulated body fluid

Punnama Siriphannon[a,1], Yoshikazu Kameshima[a], Atsuo Yasumori[a], Kiyoshi Okada[a,*], Shigeo Hayashi[b]

[a]*Department of Inorganic Materials, Tokyo Institute of Technology, O-okayama, Meguro, Tokyo 152-8552, Japan*
[b]*Research Institute of Materials and Resources, Mining College, Akita University, Tegatagakuen, Akita 010-8502, Japan*

Received 10 January 2001; received in revised form 10 April 2001; accepted 21 April 2001

Abstract

$CaSiO_3$ powders were prepared from ethanol solutions of $Ca(NO_3)_2{\cdot}4H_2O$ and $Si(OC_2H_5)_4$ using NaOH as a precipitant. The resultant powders were heated at three different temperature regimes, (1) 500°C, (2) 500 and 1000°C and (3) 500 and 1400°C, to obtain the amorphous phase (amorphous-CS), low temperature phase (β-CS), and high temperature phase (α-CS) of $CaSiO_3$, respectively. The different amorphous and crystalline phases exhibited different microtextures and specific surface areas of the powders. The rough, porous particles of amorphous-CS and β-CS have higher specific surface areas than the smooth, dense particles of α-CS. These $CaSiO_3$ powders were soaked in a simulated body fluid (SBF) at 36.5°C for 2 h to 30 days. Formation of hydroxyapatite (HAp) was observed on the surfaces of all samples, but the formation behavior and microstructures were different, resulting the differences in microstructure and crystal structure of the starting powders as well as particle size and specific surface area. The HAp formed on the amorphous-CS was a loose porous layer consisting of uniformly-sized tiny ball-like agglomerated particles, while that formed on the β-CS and α-CS was a dense layer consisting of larger ball-like agglomerated particles.

Keywords: Apatitie; Bioactive materials; $CaSiO_3$ powders; Simulated body fluid (SBF)

1. Introduction

During the last four decades, various materials known as 'bioactive materials' such as glasses,[1–3] sintered hydroxyapatite,[4] glass ceramics,[5–7] composite materials,[8–10] etc., have been synthesized and developed for medical applications. A significant characteristic of bioactive materials is their ability to bond with living bone through the formation of a hydroxyapatite (HAp) interface layer. The same HAp layer is reported to form on the surfaces of bioactive materials after soaking in a biomimetic system of simulated body fluid (SBF) which has ion concentrations similar to human blood plasma. The proposed mechanism of HAp formation involves the dissolution of calcium ions from the bioactive materials into the body fluid, with the simultaneous formation of a silica-rich interlayer on the material surfaces. The dissolution of the calcium ion increases the degree of supersaturation of the surrounding fluid with respect to HAp, while the silica-rich interlayer provides favorable sites for HAp nucleation by dissolving an appreciable amount of silicate ion.[11–13] The nucleation and growth of the HAp layer proceeds by reaction of the calcium, phosphate, and hydroxide ions from the surrounding fluid,[2,3,13–15] sometimes incorporating with carbonate or fluoride anions.[2,14,16–19]

α-$CaSiO_3$ ceramics prepared from coprecipitated powders using NaOH as the precipitant have been proposed as new candidate bioactive materials by the present authors since they can induce the fast formation of an HAp layer after soaking in SBF solution.[20–22] It is believed that the presence of calcium and silicate ions in the α-$CaSiO_3$ ceramics plays an important role in the formation of HAp.[23]

The present study investigates the effect of the structure of the $CaSiO_3$ powders on the formation behavior of HAp by soaking various amorphous and crystalline $CaSiO_3$ powders in a SBF solution for varying periods.

* Corresponding author.
E-mail address: kokada@ceram.titech.ac.jp (K. Okada).
[1] Present address: Department of Chemistry, Faculty of Science, King Mongkut's Institute of Technology Ladkrabang, Chalongkrung Road, Ladkrabang, Bangkok 10520, Thailand.

0955-2219/02/$ - see front matter
PII: S0955-2219(01)00301-6

2. Experimental

2.1. Preparation of $CaSiO_3$ powders

$CaSiO_3$ powder was prepared by coprecipitation, using $Ca(NO_3)_2{\cdot}4H_2O$ and $Si(OC_2H_5)_4$ (TEOS) as the raw materials. These reagents were dissolved in 500 ml of ethanol, the concentration was adjusted to 0.2 mol/l, and the solution was stirred for 2 h. Precipitation was obtained by adding 0.33 mol/l NaOH solution to the solution. The precipitated gel was filtered, washed once with distilled water, dried in an oven at 100°C overnight, and calcined at 500°C for 2 h. The chemical composition of the as-prepared powder determined by X-ray fluorescence (XRF; RIX3000, Rigaku Co., Tokyo, Japan) was CaO 46.2, SiO_2 53.4, and Na_2O 0.4 mass% on a dry-weight basis.

The calcined powder (amorphous $CaSiO_3$) was divided into three parts and subjected to different firing processes as follows; (1) fired at 1000°C for 2 h to obtain the low temperature crystalline phase β-$CaSiO_3$ and (2) fired at 1400°C for 2 h to obtain the high temperature phase α-$CaSiO_3$. The resultant powders are, hereafter, designated amorphous-CS, β-CS, and α-CS. The powders were sieved to 24–100 mesh (710–124 μm) before being used for the soaking experiments. The specific surface areas of the powders were calculated by the BET method based on N_2 gas adsorption isotherms measured at −196°C (Autosorb-1, Quantachrome Co., FL, USA).

2.2. Soaking in simulated body fluid

The simulated body fluid (SBF) was prepared by dissolving reagent-grade $CaCl_2$, $K_2HPO_4{\cdot}3H_2O$, NaCl, KCl, $MgCl_2{\cdot}6H_2O$, $NaHCO_3$ and Na_2SO_4 in distilled water and adjusting the ion concentrations to be similar to those in human blood plasma (Table 1).[6,7] The SBF solution was buffered at pH 7.25 with tris–(hydroxymethyl)-aminomethane [$(CH_2OH)_3CNH_2$] and hydrochloric acid (HCl). The $CaSiO_3$ powders were soaked in the SBF solution using the corresponding containers for 2 h, and 1, 5, 10, 15, 20, 25 and 30 days at a solid/liquid ratio of 1 mg/ml.[10] The soaking experiment was carried out in a shaking bath maintained at 36.5°C (human body temperature). After the pre-selected soaking time, the powders were filtered off, rinsed in distilled water and dried at room temperature. The soaking experiment was done only once for amorphous-CS, β-CS and α-CS, respectively.

Table 1
Ion concentrations of simulated body fluid and human blood plasma

	Ion concentration (mM)						
	Na^+	K^+	Mg^{2+}	Ca^{2+}	C^{1-}	HCO_3^-	HPO_4^{2-}
Simulated body fluid	142.0	5.0	1.5	2.5	148.8	4.2	1.0
Blood plasma	142.0	5.0	1.5	2.5	103.0	27.0	1.0

2.3. Analysis of hydroxyapatite (HAp) formation

The soaked and dried $CaSiO_3$ powders were crushed in an agate mortar to fine powders and investigated by X-ray diffractometry (XRD; Geigerflex, Rigaku Co., Tokyo, Japan) using monochromated CuK_α radiation and Fourier transform infrared spectroscopy (FTIR; 8000PC, Shimadzu Co., Kyoto, Japan). The microstructures of the soaked powders were observed by scanning electron microscopy (SEM; s-2050, Hitachi Ltd., Tokyo, Japan). The concentrations of Ca, Si, and P in the SBF solution after soaking the $CaSiO_3$ powders were determined by inductively coupled plasma atomic emission spectroscopy (ICP; SPS1500VR, Seiko Instruments Inc., Tokyo, Japan). For these analyses, 5 ml of the spent solution was diluted to 50 ml with distilled water.

3. Results and discussion

3.1. Characteristics of $CaSiO_3$ powders

Fig. 1 shows the XRD patterns (a) and SEM micrographs (b) of the three $CaSiO_3$ powders. The XRD pattern of the amorphous-CS showed a broad peak (halo) at about 30° 2θ, while the patterns of the β-CS and α-CS confirmed the presence of crystalline β-$CaSiO_3$ and α-$CaSiO_3$, respectively. Fig.1(b) shows the surface of both the amorphous-CS and the β-CS to be rough, but the α-CS was smooth, consisting of elongated α-$CaSiO_3$ grains with a very thick glassy phase at the grain boundaries. The chemical composition of this grain boundary glassy phase is considered to be silica-rich, since the product of its partial devitrification (cristobalite) is observed at 22° 2θ in the XRD pattern. The specific surface area was 12.2 and 7.9 m^2/g in the amorphous-CS and β-CS, respectively, but was below the measurable value (1 m^2/g) in the α-CS.

The above results indicate that the increased firing temperature caused the powder particles to densify, especially in the α-CS in which it was assisted by formation of a liquid phase. This resulted in a different microstructure of the α-CS powder particles and a decrease in their specific surface area.

3.2. Characteristics of the formed HAp

3.2.1. XRD and FTIR

Figs. 2–4 show the XRD patterns and FTIR spectra of the amorphous-CS, β-CS, and α-CS samples before and after soaking in the SBF solution. The XRD and FTIR data were measured after crushing the soaked

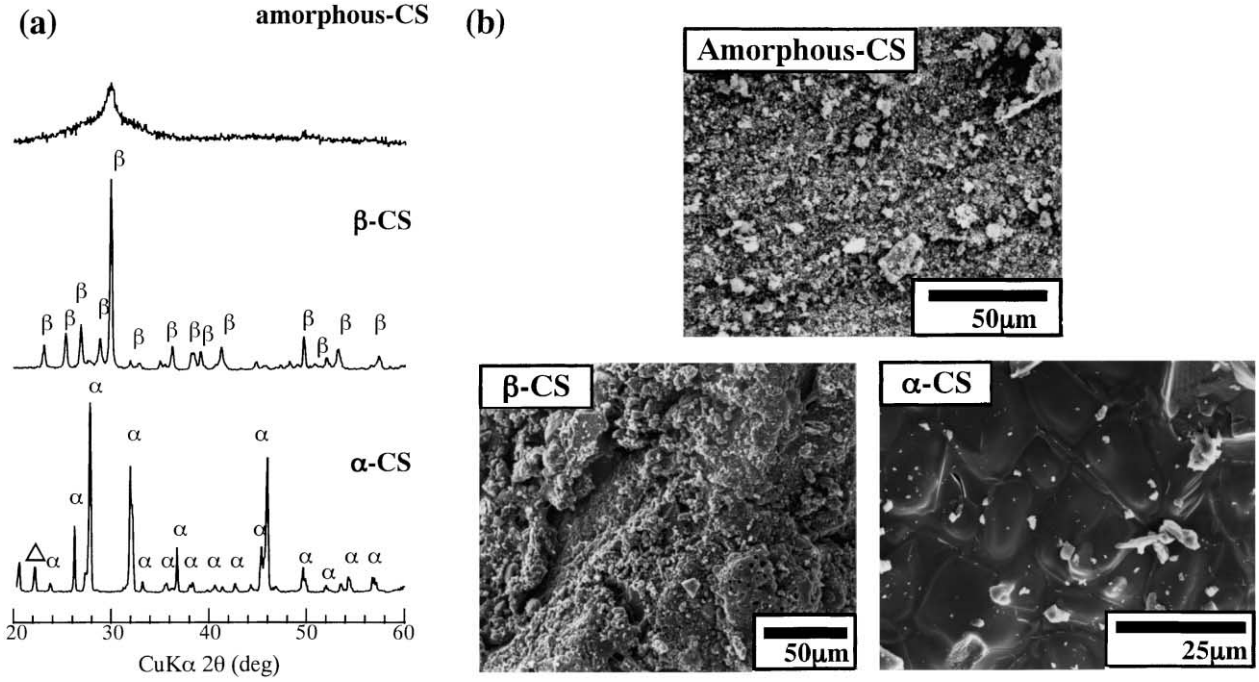

Fig. 1. XRD patterns of (a) three $CaSiO_3$ powders and (b) SEM micrographs of these as-prepared powders. β: β-$CaSiO_3$ (low temperature phase); α: α-$CaSiO_3$ (high temperature phase); △: cristobalite.

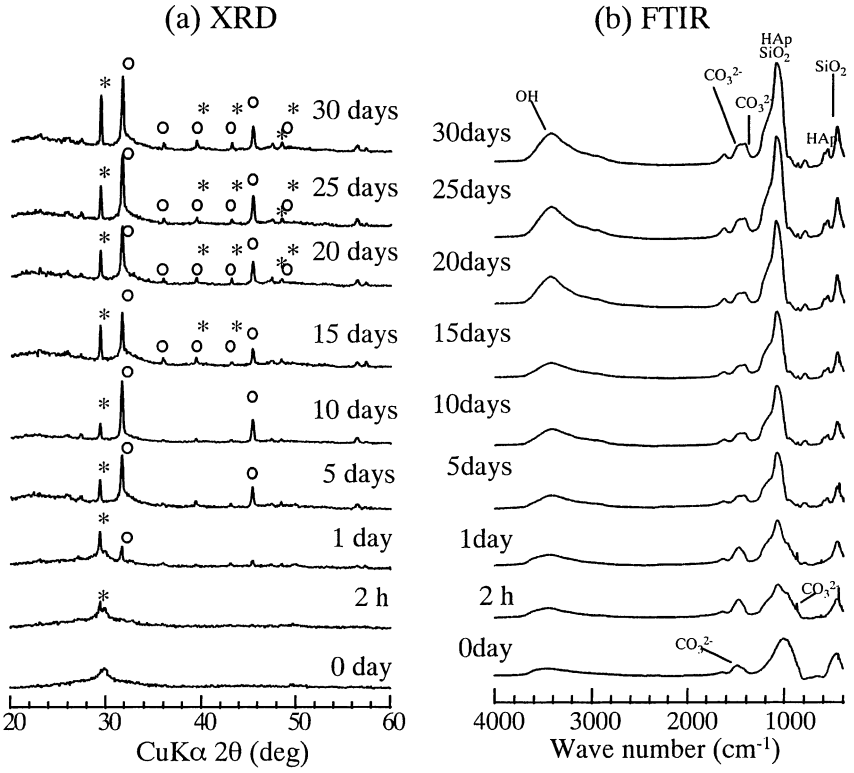

Fig.2. (a) XRD patterns and (b) FTIR spectra of the amorphous-CS before and after soaking in SBF solution; ∗: calcite; ○: HAp.

powders; these data, therefore, show the bulk constituent phases in the samples and not just the surface. Table 2 shows the assignments of the FTIR absorption bands.

In the amorphous-CS, a crystalline XRD peak observed at 29.3° 2θ [Fig. 2(a)] after soaking for 2 h was identified as calcite ($CaCO_3$). This is thought to be caused by the crystallization of an amorphous $CaCO_3$

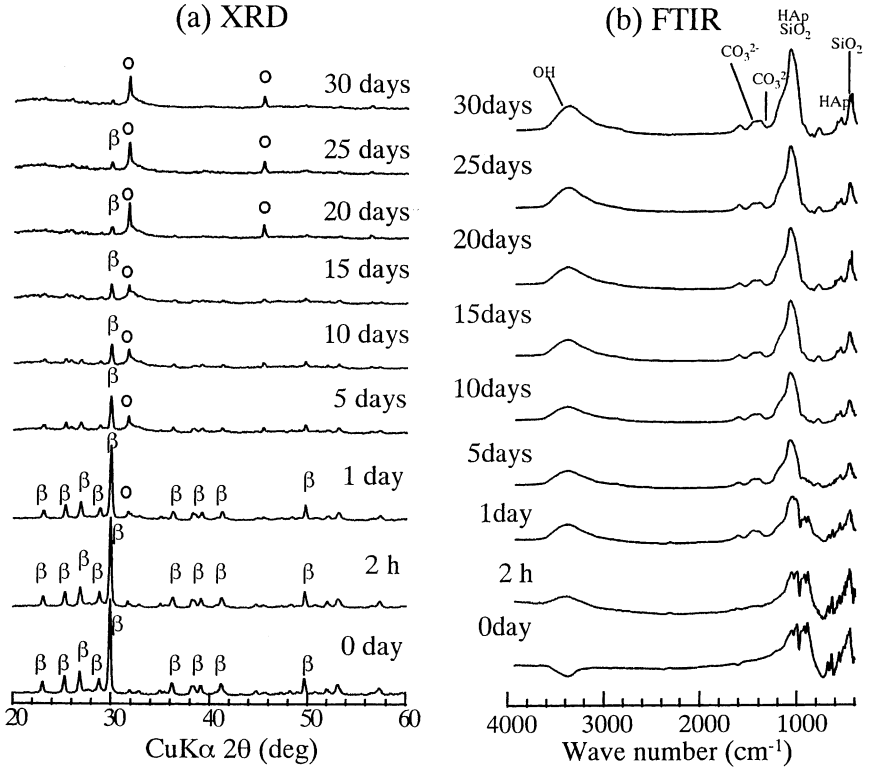

Fig. 3. (a) XRD patterns and (b) FTIR spectra of the β-CS before and after soaking in SBF solution. β: β-$CaSiO_3$; ○: HAp.

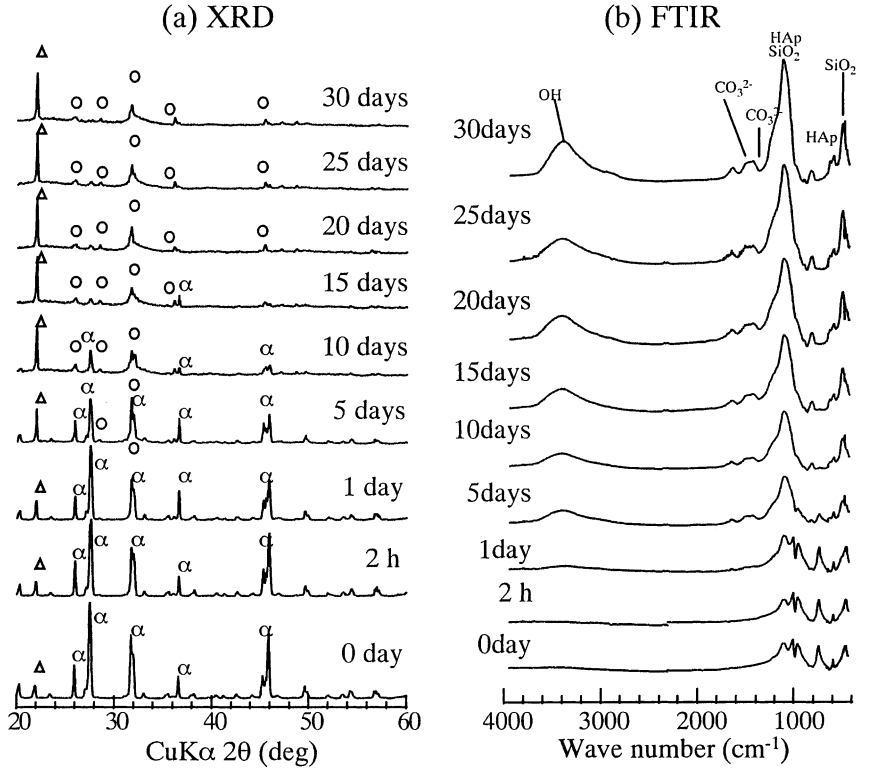

Fig. 4. (a) XRD patterns and (b) FTIR spectra of the α-CS before and after soaking in SBF solution. α: α-$CaSiO_3$; △: cristobalite; ○: HAp.

constituent of the original amorphous-CS. The FTIR C–O absorption band corresponding to this amorphous $CaCO_3$ was detected at about 1485 cm^{-1} in the spectrum of the amorphous-CS prior to soaking. HAp formation was however detected in the FTIR spectrum of the 2 h soaked sample [Fig. 2(b)] as a composite

Table 2
Assignment for FTIR absorption bands (cm^{-1}) of the $CaSiO_3$ powders after soaking in the SBF solution

Absorption band (cm^{-1})					Band assignment
Amorphous-CS	β-CS	α-CS	Calcium hydroxyapatite[17]	Carbonate hydroxyapatite[19]	
3429	3440	3450	3572	No report	O–H stretching
1415–1500	1415–1500	1415–1512	–	–	C–O stretching of CO_3^{2-} substitution for PU_4^{3-} and/or OH^-
1080 ► 1093	1093	1093	1087, 1046	1037.6	P–O stretching of HAp (υ_3) Si–O stretching of silica-rich phase
953	952	953	962	958.2	P–O stretching of HAp (υ_1)
875	870	877	–	873.7	C–O stretching of CO_3^{2-} substitution for PO_4^{3-} and/or OH^-
800	800	800	No report	No report	Si–O–Si stretching (tetragonal)[2]
606	605	609	601	602.3	O–P–O bending of HAp (υ_4)
567	567	565	571	563.9	O–P–O bending of HAp (υ_4)
468	468	466	474	464	O–P–O bending of HAp (υ_2) and/or Si–O–Si bending[14]

absorption band at about 1080 cm^{-1}, composed of the P–O stretch of HAp and the Si–O vibration of the silica-rich phase, superimposed on the silicate absorption band of the starting powder (991 cm^{-1}). A crystalline peak of HAp at 31.7° 2θ corresponding to the *211* reflection was clearly observed in the XRD pattern after 1 day soaking. After prolonged soaking the HAp peaks became the main constituent of the XRD patterns as the HAp content increased and completely covered the surfaces of the powders, but strong peaks of calcite were also observed. These calcite peaks must arise from the $CaCO_3$ residue inside the powder grains because these were crushed after the soaking experiments and before the XRD measurements. Anyway, co-existence of $CaCO_3$ in the amorphous-CS may be disadvantage point for biomedical application because it is considered to show negative effect in vivo. The presence of calcite was not observed in the other two samples because the carbonate was completely removed from the β-CS and α-CS during firing. In addition, the FTIR spectra show the characteristic bands of HAp at about 1093 (shifted from 1080 cm^{-1}), 606, and 567 cm^{-1} and also show the absorption bands at about 875 and 1415–1500 cm^{-1} of carbonate which is thought to be incorporated into the HAp. These vibrational modes of carbonate are typical of carbonate groups substituting for the phosphate (PO_4^{3-}) and/or hydroxide (OH^-) groups in the HAp structure.[18]

In the β-CS, the *211* peak of HAp started to appear in the XRD pattern [Fig. 3(a)] after 1 day soaking although the β-$CaSiO_3$ peak at 30° 2θ was still observed even after prolonged soaking. This result indicates that β-$CaSiO_3$ still remains in the powder even after the surfaces are completely covered by the layer of HAp. The intensities of the HAp peaks in the β-CS are lower than in the amorphous-CS, suggesting that the crystallinity of HAp on the β-CS may be lower than that on the amorphous-CS. The FTIR spectra of Fig. 3(b) show a combination of the P–O absorption bands of the HAp, the Si–O absorption bands of the silica-rich phase, and the C–O absorption bands of the carbonate group which occur in almost the same positions.

The α-$CaSiO_3$ peak at about 32° 2θ in the α-CS was broadened due to its overlap with the *211* peak of HAp after 1 day soaking [Fig. 4(a)]. The main XRD peaks in this sample gradually changed from α-$CaSiO_3$ to HAp until the α-$CaSiO_3$ peaks were no longer detectable in the samples soaked for prolonged times. At the same time, the intensity of the cristobalite peak at $2\theta = 22^o$ increased with increasing soaking time, indicating that although the α-$CaSiO_3$ grains dissolved completely in the SBF solution, the cristobalite did not dissolve even after prolonged soaking. The intensity increase of cristobalite is therefore due to a relative condensation effect. These results are quite different from the other two samples, probably because of differences in the microstructure of the starting powders. The FTIR spectra of Fig. 4(b) showed a change from the silicate absorption bands of the starting α-$CaSiO_3$ to the P–O absorption bands of HAp, superimposed on the Si–O absorption bands of the silica-rich phase, and the C–O absorption bands of the carbonate group (Table 2).

These results suggest a mechanism of HAp formation on the $CaSiO_3$ powders involving its initiation from a rapidly-formed silica-rich interlayer, followed by the formation of an amorphous calcium phosphate layer resembling HAp by reaction of Ca^{2+}, PO_4^{3-} and OH^- ions from the SBF solution. After the prolonged soaking, the amorphous layer grows and crystallizes to HAp with partial incorporation of CO_3^{2-} which may be related to the low crystallinity and small crystallite size of the HAp.

3.2.2. Microstructure of the formed HAp

Figs. 5–7 show SEM micrographs of the surfaces of the amorphous-CS, β-CS, and α-CS after soaking in the SBF solution for various times. In the amorphous-CS, tiny ball-like agglomerated particles thought to be HAp were observed on the surface of the sample soaked for 2 h (Fig. 5). At longer soaking times, the number of agglomerated HAp particles increases with the formation of tiny new ball-like HAp particles rather than by growth in the size of the HAp particles already present. The surfaces of the long-soaked samples are covered with these tiny ball-like HAp particles. The texture of this layer consists

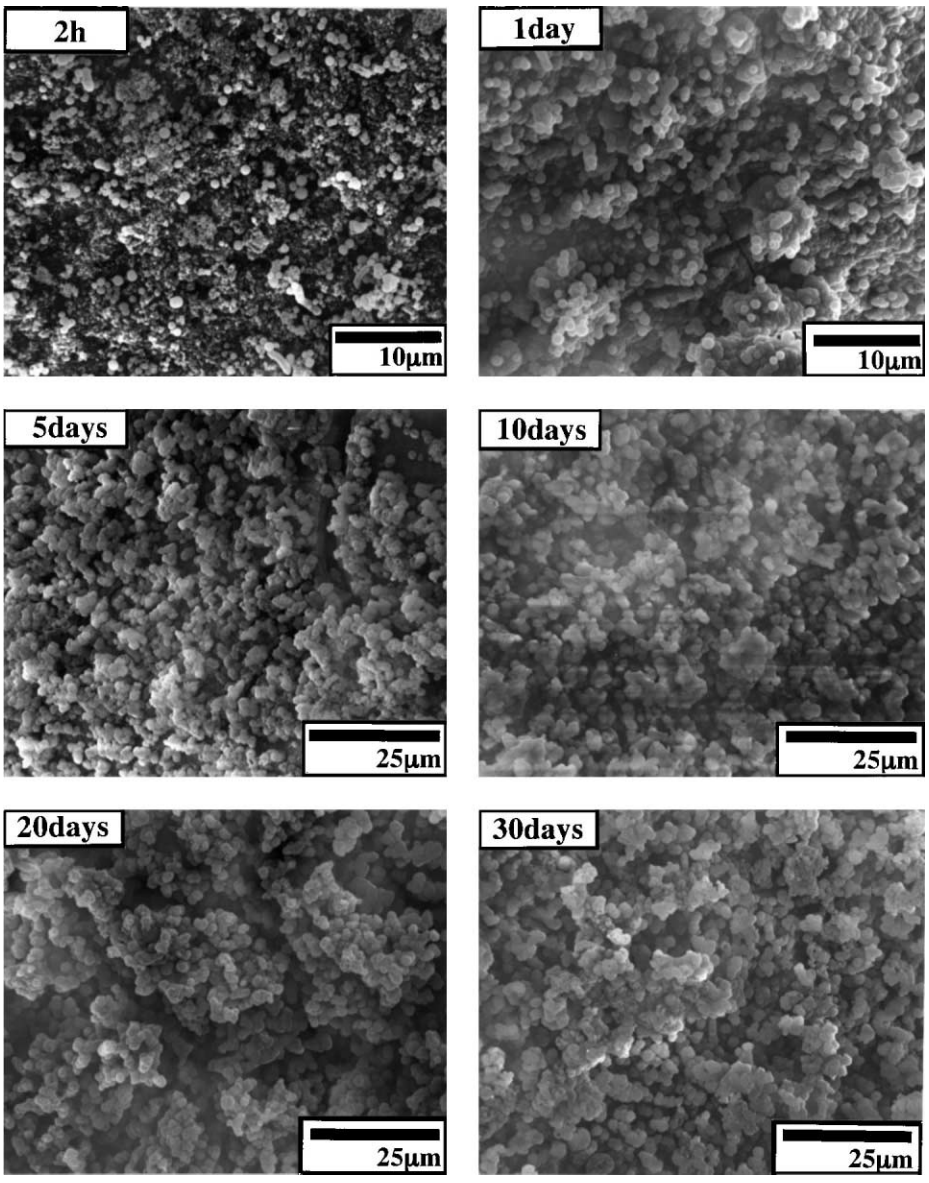

Fig. 5. SEM micrographs of the surfaces of amorphous-CS after soaking in the SBF solution for various times.

of loosely packed agglomerates presenting a rough surface. The formation of this HAp layer occurred not only on the surface of the amorphous-CS, but also on the surface of the polypropylene container. This phenomenon did not occur in the soaking experiments with β-CS or α-CS. Fig. 8 shows a SEM micrograph (a) and XRD pattern (b) of the HAp formed on the surface of the container after soaking the amorphous-CS for 5 days. This HAp occurs as porous spherical particles composed of flake-like crystals. This unique texture gives rise to preferred orientation in the XRD pattern manifested as strong intensities of the *211*, *222*, and *322* HAp reflections. The high crystallinity of the HAp formed in this sample is also thought to be related to this phenomenon.

Figs. 6 and 7 show the HAp formed on the surfaces of both β-CS and α-CS powders after 1 day soaking to occur as a dense layer consisting of tiny ball-like particles. On soaking for longer times, the HAp formed on both the β-CS and α-CS grew both as a result of increasing particle size and also with the formation of new HAp particles on the surfaces of other particles. Corresponding to the differences in growth behavior of these three samples, the HAp layers formed on the β-CS and α-CS surfaces appear denser than those on the amorphous-CS surfaces. The size of the product HAp particles decreased in the order α-CS > β-CS > amorphous-CS.

Although a strong cristobalite XRD peak was observed in the soaked α-CS [Fig. 4(a)], no cristobalite particles were found in the SEM photographs of these samples. This result indicates that the cristobalite observed by XRD came from the original powder and was not formed during the soaking experiment.

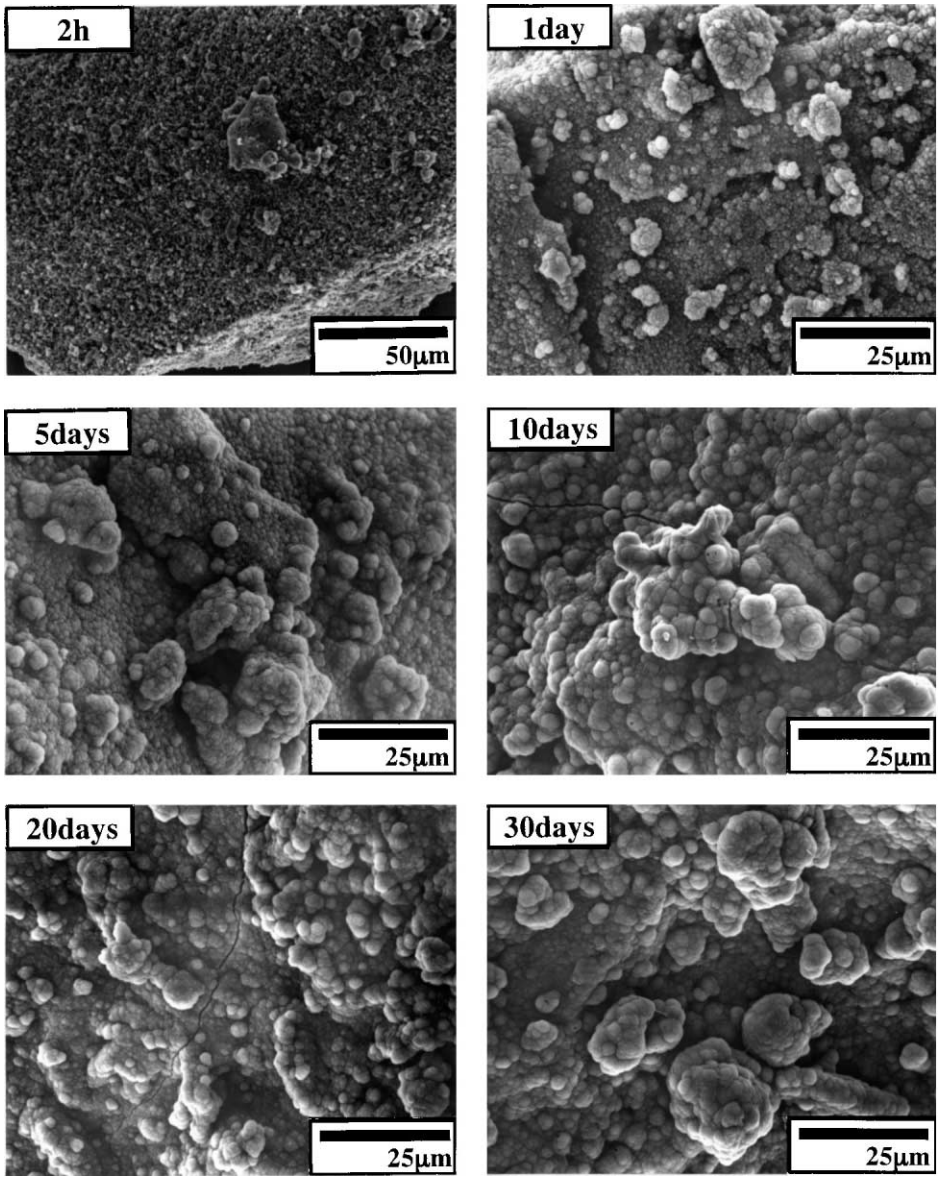

Fig. 6. SEM micrographs of the surfaces of β-CS after soaking in the SBF solution for various times.

The above results show that the differences in formation behavior and microstructure of the product HAp layer arise from differences in the microstructure, surface area, and $CaSiO_3$ phase of the starting powders.

3.2.3. Concentration changes of the SBF solution

Fig. 9 shows the change in concentration of Ca, Si, and P in the SBF solution measured by ICP after soaking the three $CaSiO_3$ powders for various times. During the early stages of soaking, the Ca and Si concentrations in the SBF solution increase steeply with a corresponding steep decrease in the P concentration. This reflects the dissolution of the powder surfaces with a simultaneous uptake of P from the solution into the powders.

The amorphous-CS showed the highest release of Ca into the SBF solution but a lower release of Si than from the other two samples. It is considered that the firing temperature of 500°C was insufficient for complete reaction of the CaO and SiO_2 components of the amorphous-CS to form $CaSiO_3$. The unreacted CaO may then carbonate to amorphous $CaCO_3$ by reacting with CO_3^{2-} in the SBF solution as suggested by the FTIR spectrum of the amorphous-CS [Fig. 2(b)]. The unreacted CaO and/or amorphous $CaCO_3$ in the amorphous-CS are thought to dissolve faster in the SBF solution than either the SiO_2, β-$CaSiO_3$ or α-$CaSiO_3$ phases. The higher release of Ca from the amorphous-CS caused a more rapid increase in the pH of the SBF solution, resulting in the faster precipitation of HAp with the consumption of the Ca^{2+}, PO_4^{3-}, and OH^- as reflected by the steep decrease in the P concentration of the solution.

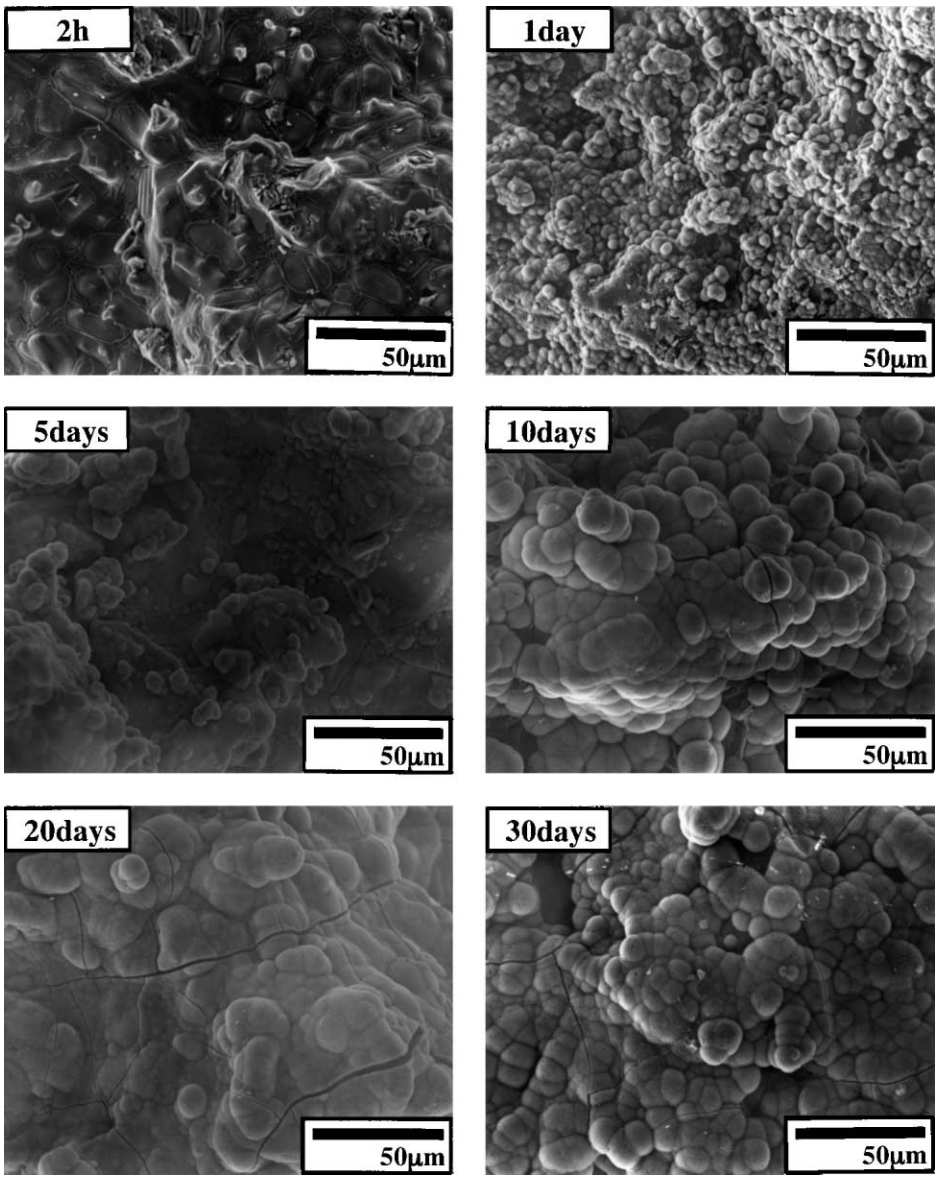

Fig. 7. SEM micrographs of the surfaces of α-CS after soaking in the SBF solution for various times.

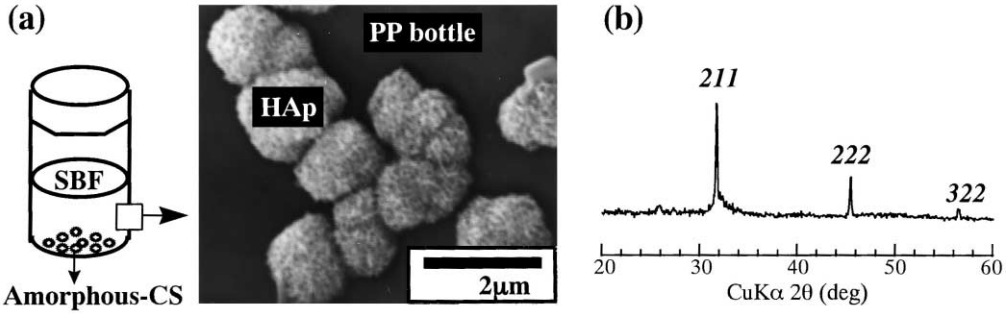

Fig. 8. (a) SEM micrograph and (b) XRD pattern of the HAp layer formed on the surface of soaking container (PE bottle) after soaking with the amorphous-CS for 5 days.

After prolonged soaking, the Ca concentration is similar in the solutions from amorphous-CS and β-CS, but is higher in the α-CS solution. This is due to the complete dissolution of α-$CaSiO_3$, but not the β-$CaSiO_3$ and $CaCO_3$ of the other samples. The Si and P concentrations also showed differences between the samples, for reasons which are not presently understood. After prolonged soaking, the Ca, Si, and P concentrations

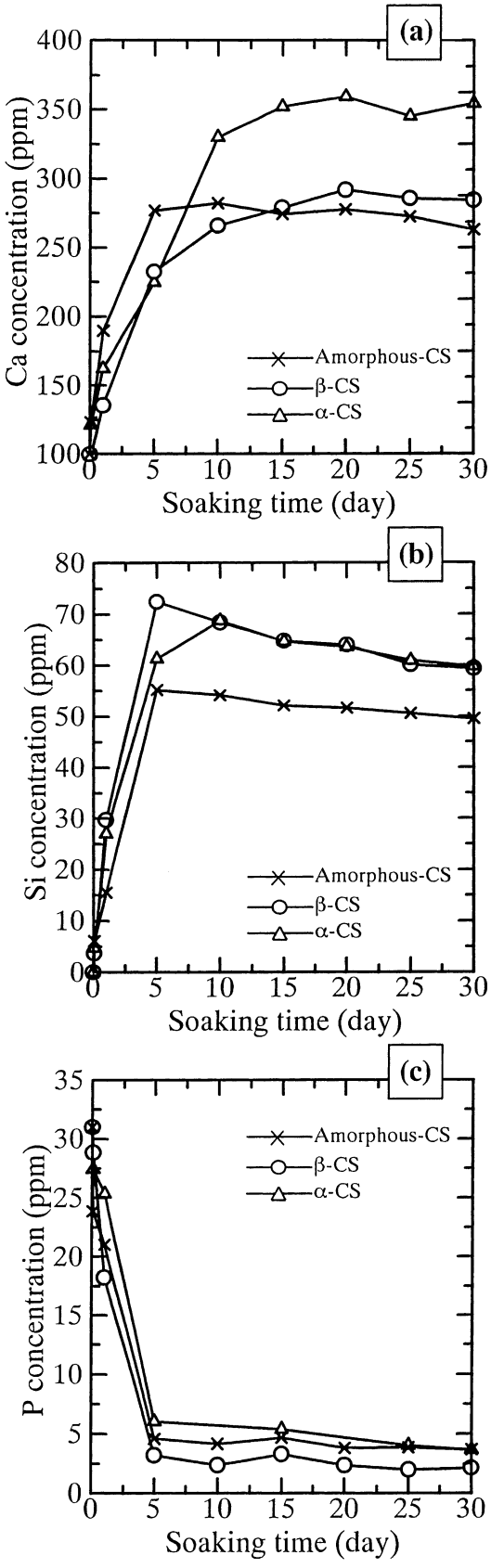

Fig. 9. Changes of Ca, Si, and P concentrations of the SBF solution after soaking with the $CaSiO_3$ powders for various times.

became almost constant, indicating an apparent equilibrium state between the dissolution of the powder surfaces and the formation of HAp.

4. Conclusions

1. $CaSiO_3$ powders with different amorphous and crystalline phases showed differences in their microstructure and specific surface area. Rough, porous particles composed of aggregated fine particles occurred in amorphous-CS and β-CS and had higher specific surface areas than the smooth densely aggregated particles of α-CS.

2. These differences in microstructure and specific surface areas of the starting $CaSiO_3$ powders influenced the formation behavior, microstructure, and particle size of the HAp formed on their surfaces after soaking in SBF solution. The HAp layer formed on the amorphous-CS was of a rough and loose texture, consisting of uniformly sized tiny ball-like particles, whereas a denser layer of larger particle size was formed on the β-CS and α-CS.

3. Amorphous-CS showed the fastest formation of HAp due to the rapid release of Ca. This product was however highly contaminated with $CaCO_3$ which crystallized from the amorphous $CaCO_3$ present in the starting powder.

Acknowledgements

A part of this work was financially supported by the Japan Society for the Promotion of Science (Project: Preparation of Advanced Inorganic Materials by Soft, Solution Processing). We are also grateful to Dr. K.J.D. MacKenzie for critical reading and editing of the manuscript.

References

1. Hench, L. L., Splinter, R. J., Allen, W. C. and Greenlee, T. K., *J. Biomed. Mater. Res. Symp.,* 1971, **2**, 117.
2. Hench, L. L. J., *Am. Ceram. Soc.,* 1991, **74**, 1487.
3. Hench, L. L. and Andersson, O., *An Introduction to Bioceramics.* World Scientific, Singapore, 1993.
4. Jarcho, M., Kay, J. F., Gumaer, K. I., Doremus, R. H. and Drobeck, H. P., *J. Bioeng.,* 1977, **1**, 79.
5. Kokubo, T., Shigematsu, M., Nagashima, Y., Tashiro, M., Nakamura, T., Yamamuro, T. and Higashi, S., *Bull. Inst. Chem. Res.,* 1982, **60**, 260.
6. Kokubo, T., *J. Non-Cryst. Solids,* 1990, **120**, 138.
7. Kokubo, T., *An Introduction to Bioceramics.* World Scientific, Singapore, 1993.
8. Ducheyne, P., Raemdonck, W. V., Heughebaert, J. C. and Heughebaert, M., *Biomaterials,* 1986, **7**, 97.
9. Santos, J. D., Jha, L. J. and Monteiro, F. J., *J. Mater. Sci.: Mater. Med.,* 1996, **7**, 181.
10. Falaize, S., Radin, S. and Ducheyne, P., *J. Am. Ceram. Soc.,* 1999, **82**, 969.

11. Kokubo, T., *J. Ceram. Soc. Japan,* 1991, **99**, 965.
12. Kokubo, T., Kushitani, C., Ohtsuki, C., Sakka, S. and Yamamuro, T., *J. Mater. Sci.: Mater. Med.,* 1993, **4**, 1.
13. Cho, S. B., Miyaji, F., Kokubo, T., Nakanishi, K., Soga, N. and Nakamura, T., *J. Biomed. Mater. Res.,* 1996, **32**, 375.
14. Kim, C. Y., Clark, A. E. and Hench, L. L., *J. Non-Cryst. Solids,* 1989, **113**, 195.
15. Cho, S. B., Nakanishi, K., Kokubo, T., Soga, N., Ohtsuki, C. and Nakamura, T., *J. Biomed. Mater. Res.,* 1996, **33**, 145.
16. LeGeros, R. Z., Trautz, O. R., LeGeros, J. P. and Klein, E., *Bull. Soc. Chim. France*, 1968, 1712.
17. Fowler, B. O., *Inorg. Chem.,* 1974, **13**, 194.
18. Arends, J. and Davidson, C. L., *Calcif. Tiss. Res.,* 1975, **18**, 65.
19. Vallet-Regi, M., Romero, A. M., Ragel, C. V. and LeGeros, R. Z., *J. Biomed. Mater. Res.,* 1999, **44**, 416.
20. Siriphannon, P., Hayashi, S., Yasumori, A. and Okada, K., *J. Mater. Res.,* 1999, **14**, 529.
21. Siriphannon P., Kameshima, Y., Yasumori, A. and Okada, K. In *Bioceramics 12*, ed. H. Ohgushi, G. W. Hastings and T. Yoshikawa. World Scientific, Singapore, 1999, pp. 145–148.
22. Siriphannon, P., Kameshima, Y., Yasumori, A., Okada, K. and Hayashi, S., *J. Biomed. Mater. Res.,* 2000, **52**, 30.
23. Li, P., Ohtsuki, C., Kokubo, T., Nakanishi, K., Soga, N., Nakamura, T. and Yamamuro, T., *J. Mater. Sci.: Mater. Med.,* 1993, **4**, 127.